Work of adhesion of interfaces between M_2AlC (M=Ti, V, Cr) MAX phases and α-Al_2O_3

Kwakernaak, Cees; Sloof, Willem G.

DOI
10.1016/j.ceramint.2018.09.127

Publication date
2018

Document Version
Accepted author manuscript

Published in
Ceramics International

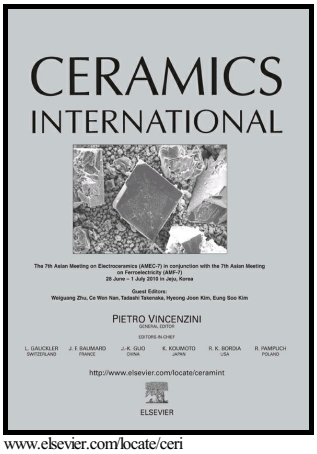

www.elsevier.com/locate/ceri

Work of Adhesion of interfaces between M_2AlC (M = Ti, V, Cr) MAX phases and α-Al_2O_3

Cees Kwakernaak, Willem G. Sloof

PII: S0272-8842(18)32592-6
DOI: https://doi.org/10.1016/j.ceramint.2018.09.127
Reference: CERI19526

To appear in: *Ceramics International*

Received date: 14 August 2018
Revised date: 28 August 2018
Accepted date: 13 September 2018

Cite this article as: Cees Kwakernaak and Willem G. Sloof, Work of Adhesion of interfaces between M_2AlC (M = Ti, V, Cr) MAX phases and α-Al_2O_3, *Ceramics International,* https://doi.org/10.1016/j.ceramint.2018.09.127

Work of Adhesion of interfaces between M_2AlC (M = Ti, V, Cr) MAX phases and α-Al_2O_3

Cees Kwakernaak[1], Willem G. Sloof

Delft University of Technology, Department of Materials Science and Engineering, 2628 CD Delft, The Netherlands.

Abstract:

A fast and generic scheme is proposed to calculate the work of adhesion between two different materials or the cohesive energy between two crystal planes in a material. These calculations make use of the regular solution theory. This theory is extended to describe chemical interactions between atoms at either side of an interface. The so-called regular solution parameter is estimated from thermodynamic values tabulated or solution enthalpies obtained from a macroscopic atom model (MAM). Complex surface definitions at either side of an interface, both in composition and position of atoms, can be dealt with.

The proposed scheme has been used to calculate the work of adhesion between M_2AlC (M = Ti, V, Cr) type MAX phases and α-Al_2O_3. Next, the cohesive energy of the MAX-phases and alumina were determined. The cohesion of the M_2AlC type MAX-phase is the weakest bond present in the M_2AlC- α-Al_2O_3 systems.

Keywords:

work of adhesion, cohesive energy, interfaces, surfaces, MAX-phases, α-alumina

[1] Corresponding author: c.kwakernaak@tudelft.nl

1. Introduction

M_2AlC (M = Ti, V, Cr) belongs to the family of MAX phase metallo-ceramics, which are tough and therefore damage tolerant compared with many other common engineering ceramics [1]. These MAX phase are stable up to high temperatures and oxidation resistant [2-5]. At high temperatures in an oxidizing environment a protective scale is formed. On Ti_2AlC and Cr_2AlC the scale is predominately composed of alumina [6, 7], but on V_2AlC the composition of the scale is more complex [8]. The high thermal conductivity of these MAX phases makes them thermal shock resistant [9, 10]. All these properties are attractive for high temperature applications, where the material is exposed to thermal cycles, mechanical loading and oxidation. It has been demonstrated that crack damage in Ti_2AlC and Cr_2AlC can be healed by oxidation filling the crack gap with the reaction products [11-16]. To restore the strength of the material and thus the structural integrity, the adhesion between MAX phase matrix and healing product should be strong.

An advanced application of MAX phases has been demonstrated in harsh turbine engine environments (cf. [17] and references therein). It is crucial to choose a good match of the coefficient of thermal expansion (CTE) between MAX phases, healing oxide and thermal barrier coating (TBC) [14, 17]. This condition was fulfilled for Ti_2AlC, which possesses a CTE matching with those of alumina and yttrium stabilized zirconia (YSZ). Furthermore, the alumina layer formed upon thermal oxidation of Ti_2AlC can withstand high fractions of water in the exhaust gas flow at about 1300 °C for up 2500 hours [17, 18]. Much of the TiO_2 formed during initial oxidation is chemically attacked and burnt off. The CTE of Cr_2AlC is larger than those of YSZ and alumina [19] and induces spallation of the protective alumina scale during cooling from operation temperature to room temperature. Some improvement was expected when the amount of sulfur present at the interface was reduced [20], but partial removal of sulfur from the Cr_2AlC [17] did not improve the adhesion between Cr_2AlC and

alumina. However, application of high purity MAX phases is an asset for further technological developments.

In this study, the adhesion between M_2AlC (M = Ti, V, Cr) MAX phases and α-Al_2O_3 is considered. These MAX phases show distinctive oxidation behavior depicting their individual chemistries. For example, oxidation of Ti_2AlC initially rutile is formed followed by a layer of alumina [12] with columnar structure at the Ti_2AlC interface [21]. Observations with transmission electron microscopy (TEM) revealed orientation relations between the grown alumina and Ti_2AlC [22]. Oxidation of Cr_2AlC, on the other hand, results in exclusive formation of an alumina layer [23, 24]. Due to the Al depletion of Cr_2AlC, a chromium carbide layer, mainly composed of Cr_7C_3, developed in between the alumina layer and Cr_2AlC substrate [25]. When oxidizing of V_2AlC at temperatures up to 650 ^oC a well adhering film of a mixture of Al_2O_3 and V_2O_5 forms [8, 26, 27]. But upon oxidation at higher temperatures a layer of only V_2O_5 forms that easily spalls off [26].

The interface adhesion can be computed with atomistic methods [28, 29] in which case the work of separation is obtained. These atomistic calculations offering detailed chemical and structural information are very attractive, but require long computation times. Moreover, full registry between the crystallographic lattices at interfaces is usually not observed. The imposed periodic boundary conditions in these computations often require that the crystal lattice of one material becomes distorted thereby introducing a systematic error in the total energy [29]. Here, a rapid generic method to determine the work of adhesion is presented which is based on the Dupré equation [30] and uses a macroscopic atom model (MAM) [20]. This model is extended to comprise specific crystallographic orientations at the interface. For example, a detailed analysis [31] using the MAM to an Al – γ-Al_2O_3 interface provided insight in the behavior of aluminum metal and oxide during the initial stages of oxidation [32].

First, the constituting equations to calculate the work of adhesion are presented. Next, the regular solution theory [33, 34] is adopted to include complex surface and interface chemistries. The adhesion of the MAX-phases M_2AlC with α-Al_2O_3 can then be described observing all interactions between metal atoms, carbon and oxygen across the interface. Metal-metal and metal-carbon interactions are to be considered when calculating the work of adhesion to describe the cohesive strength of the MAX-phase materials. The cohesion within α-Al_2O_3 is a benchmark for the adhesion of the interface between the MAX-phase and α-Al_2O_3, which is calculated for various terminations of the MAX-phases. In a similar manner, the work of adhesion can be calculated for any other interface configuration.

2. Work of adhesion

The work of adhesion between two materials *M* and *N* is given by the Dupré equation [30]:

$$W_{Ad} = -(\gamma_M^{surf} + \gamma_N^{surf}) + \gamma_{MN}^{interaction} \tag{1}$$

in which γ_M^{surf} and γ_N^{surf} are the surface energies of both materials and $\gamma_{MN}^{interaction}$ is the free energy of the interface between the two materials in contact. Analogously, when cleavage of one alloy or compound is considered, a work of cohesion, W_{coh}, can be associated with the cleavage plane. For liquids the surface energies constitute the work of cohesion, but the chemical bonds in solids produce an additional interaction term. The work of cohesion for one material *M* is defined as:

$$W_{Coh,M} = -(\gamma_{M,1}^{surf} + \gamma_{M,2}^{surf}) + \gamma_{M,12}^{interaction}. \tag{2}$$

The indexes refer to both sides of the cleavage plane. In case the material is crystalline, the interface at cleavage is straightforward, as the crystal structures on both sides have full registry.

The surface energy (see Appendix A) of each side *s (s=1,2)* of material *M*, i.e. $\gamma_{M,s}^{surf}$, is taken as the sum [20] of the surface enthalpy ΔH_i^{surf} of element *i* that constitutes the interface weighted by the molar surface density $n_{i(M,s)}^{surf}$:

$$\gamma_{M,s}^{surf} = \sum_i n_{i(M,s)}^{surf} \Delta H_i^{surf} \,. \tag{3}$$

As both sides of cleavage plane might possess a slightly different chemical composition, the values of $n_{i(M,s)}^{surf}$ must be distinguished. The values tabulated [35, 36] for ΔH_i^{surf} are taken with respect to the first monolayer. However, the inclusion of a subsurface layer in this model requires a modified approach to compute the surface energy; cf. Appendix A.

The chemical interactions $\gamma_{M,12}^{interaction}$ and $\gamma_{MN}^{interaction}$ concerns only neighboring atoms as in the regular solution theory [33]. Considering the atoms *i* and *j* belonging to *M* and *N* respectively, $\gamma_{MN}^{interraction}$ is described by the contact areas of interacting atoms *i* with molar surface density $n_{i(M)}^{surf}$ and atoms *j* with molar surface density $n_{j(N)}^{surf}$. As an example, an interface of two binary substances, i.e. $i = 1,2$ and $j = 1,2$, is shown in Fig. 1. The total chemical interaction energy is calculated with:

$$\gamma_{MN}^{interface} = \sum_i \sum_j \Delta H_{i(M)\text{-}j(N)}^{interaction} \tag{4}$$

where $\Delta H_{i(M)\text{-}j(N)}^{interaction}$ represents the interaction energy per unit area across the interface between all atoms *i* in *M* and *j* in *N* and calculated according to:

$$\Delta H_{i(M)\text{-}j(N)}^{interaction} = p x_{i(M)}^{surf} x_{j(N)}^{surf} \left(n_{i(M)}^{surf} \Delta H_{ij}^{sol} + n_{j(N)}^{surf} \Delta H_{ji}^{sol} \right) \tag{5}$$

where *p* is a factor describing the *partial interaction* of atoms at one side of the interface by the atoms across the interface. The interaction at the interface is smaller than for a binary substance of atoms *i* and *j*, hence $0 < p < 1$ and usually *p = 1/3* is taken [31, 35]. The

quantities $x_{i(M)}^{surf}$ and $x_{j(N)}^{surf}$ are the molar surface fraction of atoms *i* in *M* and *j* in *N*, respectively, (cf. Appendix A):

$$x_{i(M)}^{surf} = \frac{n_{i(M)}^{surf}}{\sum_{all\ i} n_{i(M)}^{surf}} \tag{6}$$

$$x_{j(N)}^{surf} = \frac{n_{j(N)}^{surf}}{\sum_{all\ j} n_{j(N)}^{surf}} \tag{7}$$

More specifically, Eq. (5) describes the interaction between atoms by a pair potential as used in regular solution theory [33]. This theory considers the interactions between atoms in direct contact in bulk materials [34, 37, 38] and defines the enthalpy of mixing ΔH_{ij}^{mix} according to:

$$\Delta H_{ij}^{mix} = \alpha_{ij} x_i x_j \tag{8}$$

where x_i and x_j are the molar fractions of element *i* and *j* respectively and α_{ij} is the regular solution parameter. The regular solution parameter α_{ij} can directly be obtained from the measured values of the formation enthalpy for a given substance. In case the formation enthalpy is unknown, the regular solution parameter can be estimated from the arithmetic mean of the solution enthalpies weighted by their molar fractions [39, 40], i.e.:

$$\alpha_{ij} = x_i \Delta H_{ij}^{sol} + x_j \Delta H_{ji}^{sol}\ , \tag{9}$$

where the respective solution enthalpies of ΔH_{ij}^{sol} and ΔH_{ji}^{sol}, with solute element *i* dissolved in pure element *j* and vice versa. Data on solution enthalpies are scarce, but can be estimated using a semi-empirical macroscopic atom model (MAM) [35], see Appendix B. Eq. (9) has found widespread application to estimate formation enthalpies of alloys and intermetallic compounds with the MAM model [35, 41-43].

Here, the mixing enthalpy is only describing the chemical interactions across the interface, thus a fraction *p* reduces the regular solution parameter and transforms the expression of the enthalpy of mixing into:

$$\Delta H_{ij}^{mix} = p\alpha_{ij}^{surf} x_{i(M)}^{surf} x_{j(N)}^{surf}. \tag{10}$$

Here, α_{ij}^{surf} only comprises interactions across the interface between element *i* from material *M* and element *j* from material *N*:

$$\alpha_{ij}^{surf} = (n_{i(M)}^{surf} + n_{j(N)}^{surf})(\xi_{i(M)}\Delta H_{ij}^{sol} + \xi_{j(N)}\Delta H_{ji}^{sol}) \tag{11}$$

and in this case the molar surface fractions $\xi_{i(M)}$ and $\xi_{j(N)}$ equals, respectively:

$$\xi_{i(M)} = \frac{n_{i(M)}^{surf}}{n_{i(M)}^{surf} + n_{j(N)}^{surf}} \tag{12}$$

and

$$\xi_{j(N)} = \frac{n_{j(N)}^{surf}}{n_{i(M)}^{surf} + n_{j(N)}^{surf}}. \tag{13}$$

which reduces Eq. (11) to:

$$\alpha_{ij}^{surf} = n_{i(M)}^{surf}\Delta H_{ij}^{sol} + n_{j(N)}^{surf}\Delta H_{ji}^{sol}. \tag{14}$$

The work of adhesion can thus be calculated for any interface given the chemical composition of both compounds and their crystallographic orientations. In the sequel, the theory presented is applied to calculate the work of adhesion of interfaces between MAX phase materials of type M_2AlC (M = Ti, V, Cr) and α-alumina. As the interfaces $M_2AlC(0001)$ – (11-20) α-Al_2O_3 and $M_2AlC(11\text{-}20)$ – (11-20) α-Al_2O_3 have been observed experimentally [12, 27], their work of adhesion is determined. Moreover, these interfaces have low index flat geometries and show the largest variation in the work of adhesion.

3. MAX phase $M_2AlC(0001)$ // (11-20) α-Al_2O_3 interface

The work of adhesion of the MAX phase – oxide systems are calculated using Eq. (1). The structure of interface of the MAX phase type M_2AlC (M = Ti, V, Cr) and α-Al_2O_3 is defined by their crystal lattices and lattice parameters (see Table 1) and their orientation with respect to each other. An example of the cross section of the interface is designated as: $M_2AlC(0001)[11\text{-}20]$ – Al // O – $[1\text{-}100](11\text{-}20)\alpha$-$Al_2O_3$ and is shown in Fig. 2, in which the MAX-phase is terminated by Al atoms and the alumina by O atoms. It is assumed that the crystal structure remains unaltered when both materials are placed opposite to each other. The work of cohesion of both materials originate from the atomic interactions across the planes indicated in Fig. 2.

The surface energies γ_M^{surf} are calculated with Eq. (3). The values of the surface energy ΔH_i^{surf} of the metals [35] were completed with those of oxygen [20] and of carbon [44, 45] with surface energy values of 0.65 eV/atom and 0.62 eV/atom, respectively. The sizes of the surface atoms determine the extent to which the atoms of the subsurface layer are obscured. The surface energies computed therefore contain the contributions of the surface and obscured subsurface atoms that are, however, partially exposed; cf. Fig. 1.

When carbon atoms terminate the MAX-phases almost all M atoms are also exposed to the surface. The small sizes of the carbon atoms cover the surface layer only partially since they lie almost embedded in the MC-layer. This is represented in the surface densities calculated, viz.: $n_C^{surf} \approx 21$ µmol/m² and $n_M^{surf} \approx 13$ µmol/m². The surface energy of the carbon layer alone equals 1.3 J/m², while the subsurface M element contributes 1.2, 1.0 and 0.85 J/m² for Ti, V and Cr, respectively. When the top surface layer consists of either Al or M elements the surface densities are about 23 µmol/m². Then, the fraction of subsurface elements is greatly reduced. The surface energy of the Al terminated planes is about 0.4 J/m² lower than the surface energy for the M element terminated plane of the MAX phases and equals 1.5 and 1.9 J/m², respectively, including the contribution of the subsurface layer.

The surface energies of alumina were calculated for the (11-20) α-Al_2O_3 planes terminated by either a single layer of oxygen or aluminum; cf. Fig 2. The aluminum plane (see Fig. 2 above the gray line) has a surface energy of 1.5 J/m², which is also found for the single oxygen layer terminated surface.

The interaction energy (see Eq. (4)) is determined by the contributions of all pair of atoms identified across the interface (see Eq. (5)). The sizes of these atoms (see Eq. (A4)) were derived from the molar surfaces computed with the MAM. The atomic radii thus obtained were used to calculate the surface fraction (see Eq. (A1)). The regular solution parameters α_{ij}^{surf} were determined using the solution enthalpies calculated with Eq. (B2). Those values were compared with experimental regular solution parameters obtained from heat of formation data of the binary compounds [46].

The calculations of the cohesive energies of the MAX phases and α-Al_2O_3 were done for coherent 'interfaces' parallel to the (0001)-plane in the MAX phases or the (11-20)-plane in α-Al_2O_3; see Table 2. The cohesive energy of α-Al_2O_3 is the largest (6.7 J/m²) and is only approached by the titanium – carbon bonds in Ti_2AlC (6.0 J/m²). The cohesive energy of the transition metal – aluminum bonds of 4.7 J/m² or less is the weakest bond in every MAX-phase considered.

The work of adhesion of the interfaces of M_2AlC with α-Al_2O_3 is presented in Table 3. The work of adhesion varies between 7.0 J/m² for Ti-terminated Ti_2AlC and 5.8 J/m² for V-terminated V_2AlC. On average, the work of adhesion between M_2AlC (0001) and Al_2O_3 (11-20) is about 6.4 J/m². The work of adhesion for the carbon terminated MAX phases is maximum 5.6 J/m² (Ti_2AlC). When the work of adhesion is compared with the cohesive energy, it becomes apparent that the carbide bonds (M-C) are stronger than the metal bonds (Al-M). Upon mechanical loading, the weakest bonds will preferentially break up. This explains why the formation of oxides recovers the strength of the MAX-phase [12, 14, 23].

4. M_2AlC(11-20) // (11-20) α-Al_2O_3 interface

When MAX phases are terminated by any (11-20)-plane the composition comprises the M element (M = Ti, V, Cr), aluminum and carbon. There is only one configuration possible within the MAX phase to calculate the cohesive energy, and thus also one configuration of the M2AlC(11-20) // (11-20) α-Al2O3 interface for determining the work of adhesion. No variations in surface compositions of either compound are present. The cohesive energies together with the surface energies of the M_2AlC(11-20) MAX phases are listed in Table 4. For Ti_2AlC and V_2AlC the cohesive energies in the (11-20)-plane are lower than those calculated for any of the interactions between the (0001)-planes; compare Tables 2 and 4. The small value of 0.3 J/m² for the interaction energy is caused by the large fraction of atoms that are identical on either side of the cleavage and for which interaction energy in the MAM reduces to zero.

The values for the work of adhesion of the interface between M_2AlC(11-20) and α-Al_2O_3(11-20) are given in Table 5. The bonding between α-Al_2O_3 and Ti_2AlC or V_2AlC is stronger than the cohesion of these MAX phases; compare Table 4 and 5. But the bonding between α-Al_2O_3 and Cr_2AlC is equal to the cohesion of Cr_2AlC, which is about 6.7 J/m².

5. Discussion

The Dupré equation [30] is applied to calculate the work of adhesion between two dissimilar surfaces and comprises both surface energies and the adhesive forces between them. This equation is widely employed in experimental studies, but is also used in thermodynamic evaluations [20, 47] in which it is assumed that equilibrium conditions apply at the interface. Experimental values obtained for W_{ad} are always too large because of dissipative effects [47]

at either side of the interface. The method described here to obtain the work of adhesion differs from that of previous work [20], in that it is now possible to include interface structure and materials with more than two elements; cf. Appendix B. The MAM computes no enthalpy effects between identical elements. This absence of interaction energy exhibits itself in the reduction of the interaction energies obtained for the (11-20) oriented MAX phases (cf. Table 4) in comparison with those obtained for the (0001) orientations (cf. Table 2).

The work of adhesion between two dissimilar materials and the cohesive energy between crystal planes within a compound are computed in the same way. The cohesive energy within one material is devoid of any mismatch effects for the material has full crystallographic registry. The crystallographic registry is often absent at interfaces of dissimilar materials and mismatch effects influence the work of adhesion. The energy associated with this accommodation of the mismatch [31, 48] is relatively small and may reduce the work of adhesion with about 0.6 J/m² at 298 K. The work of adhesion calculated in this model ignores these effects because the interface is made up of unstrained materials.

The surface energies calculated using Eq. (3) are in good agreement with earlier reported values [35, 36]. In our model, all atoms exposed to the surface contribute to the surface energy, i.e. surface and subsurface atoms. The inclusion of the subsurface layer should also be considered to accommodate non-flat surface geometries present in high-index planes. The surface energies calculated for the transition metal surfaces of the MAX-phases are approx. 2 J/m², which is comparable to those of the pure elements [35, 36]. The surface energy of carbon was indirectly obtained from literature [44, 45]. The hybridization of carbon at the surface can either result in a low or high surface energy. A high surface energy of carbon was found for broken graphite bonds and diamond with a value of about 5.0 J/m², whereas a low surface energy of 0.2 J/m² was recorded for graphite alone [44, 45]. The high surface energy obtained for the carbon atoms has been applied to the MAX phases.

The crystal orientations chosen are observed in TEM studies in which alumina forms columnar grains on top of the MAX phases considered here after prolonged oxidation. These observations confirmed the existence of orientation relations between Ti_2AlC and alumina [22] and V_2AlC and alumina [27], namely: (0001) M_2AlC // (11-20) α-Al_2O_3. Alternatively, the orientation relation (11-20) M_2AlC // (11-20) α-Al_2O_3 was also considered which has been observed as well [7, 12].

The trends observed for the cohesive energy of the (0001)-plane of the MAX phases is that M-C bonds possess a 20 % higher cohesive energy than the M-A bonds; see Table 2. Ab initio studies (cf. [49] and references therein) show that the weakest bond in the MAX phases is the A-M bond. This explains the high mobility displayed by A atoms [50, 51], which promotes the formation of the protective alumina layer and the accommodation of mechanical stresses [52]. The strong bonds between M and X elements, on the other hand, make MAX phases rigid. However, in the case of Cr_2AlC these strong bonds cause a Cr_7C_3 layer to be formed when oxidized, which suppresses the growth of an alumina scale. The strong cohesive bonds between the M-C layers result in a relatively high cohesive energy from 4.7 to 6.0 J/m²; see Table 2. The cohesive forces present in the (11-20)-orientation of the MAX-phases are slightly less than observed for the (0001)-orientations except for the Al-Cr bonds in Cr_2AlC. The cohesive energy of the (11-20)-plane of α-Al_2O_3 equals 6.7 J/m² and is thus the strongest material in the MAX-phase - alumina system. Upon high temperature oxidation of Cr_2AlCin air, a Cr_7C_3 layer develops in between the Al_2O_3 scale and the Cr_2AlC substrate [23]. However, the work of adhesion of the interfaces between Cr_2AlC and Cr_7C_3, and between Al_2O_3 and Cr_7C_3 are similar and amount to 4.3 ± 0.3 J/m² and 5.0 ± 0.4 J/m², respectively.

The work of adhesion of interfaces of M_2AlC (M = Ti, V, Cr) with α-Al_2O_3 shows that transition metals M adhere best to oxygen terminated (11-20) α-Al_2O_3 with values of 6.4 J/m², which is similar to the work of adhesion of the aluminum terminated MAX phases (6.3

J/m²). The work of adhesion is less for the carbon terminated surfaces which amounts 5.3 J/m². However, the carbon termination of the MAX phase generates the highest surface energies (2.3 J/m²). This and the fact that the volatile oxidation products CO and CO_2 will readily escape the surface, makes the carbon termination at the interface unlikely. The work of adhesion between (0001) α-Al_2O_3 and the (11-20)-oriented MAX phases is 5.9 J/m².

The work of adhesion between Cr_2AlC and alumina is about 17% lower than between Ti_2AlC and alumina. The observed spallation of the alumina on Cr_2AlC is almost absent for alumina on Ti_2AlC [17]. This behavior is completely in agreement with the assessment of crack healing of the MAX-phase by alumina. The spallation of the healing oxide is due to differences in CTE, elastic modules and work of adhesion of the MAX phases and their healing oxide [14, 17]. These properties are more favorable for Ti_2AlC than for Cr_2AlC. The work of adhesion between V_2AlC and alumina is almost equal to that of Ti_2AlC and alumina. In the case of V_2AlC the mismatch results from differences in Young's moduli only [14]. The adhesion of an α-Al_2O_3 scale on the M_2AlC (M = Ti, V, Cr) MAX phases is strong, since the work of adhesion is in between the cohesive strength of those MAX phases and alumina; see Tables 2 and 4. This is supported by the observation that when cracks are healed in Ti_2AlC by α-Al_2O_3 fracture occurs next to healed zone [12]. Thus, the strong adhesion between these MAX phases and alumina is beneficial for oxidation induced crack healing [11, 13, 14], but also for protection against high temperature oxidation by an alumina scale [53]. It suggests good Al_2O_3 scale adhesion upon high temperature oxidation as well as restoring the MAX phase material integrity when healing cracks [12].

6. Conclusions

An efficient and rapid method is presented to determine the work of adhesion between dissimilar materials and the cohesive energies within materials. The method is based on using

thermodynamic regular solution theory and macroscopic atom models. The calculations require little computational effort while complex interface configurations can be addressed. The chemical complexity of each material has been extended to contain more than 2 elements and every crystal plane can be chosen.

The surface energies computed agree well for pure metal terminations, but deviations may occur when non-metals are present near or on the surface and depend on the bond type of the non-metal element involved.

The cohesive energies calculated between crystal layers of M_2AlC (M = Ti, V, Cr) MAX-phases are lower than the work of adhesion between these MAX-phases and α-Al_2O_3. The cohesive energy of α-Al_2O_3 is the largest compared with all work of adhesions calculated.

Appendix A: Calculation of surface densities and surface energies

The surface energy $\gamma_{M,s}^{surf}$ calculated with Eq. (3) depends on the molar surface density $n_{i(M,s)}^{surf}$ of all species *i* present on the surface *s* of material *M*. The molar surface density $n_{i(M,s)}^{surf}$ is calculated with the total projected area of all atoms present on the surface and in the first subsurface layer. The inclusion of the first subsurface layer is an approach that differs from the approach used in the MAM [35]. Its inclusion enlarges the atomic surface fraction of species *i* and was considered necessary if the surface layer has an open structure. This is the case here if the first surface layer of the MAX phases consists of small carbon atoms. Then, the M element atoms of the subsurface layer make up about 50 % of the surface area. However, the molar surface enthalpy ΔH_i^{surf} that are found in literature [35, 36] were obtained for low index surfaces by only considering the atoms *i* present in the surface layer and did not consider the first subsurface layer. Inclusion of the subsurface layer results in an increase of the molar surface density and, hence, a reduction of the molar surface enthalpy. The reduction of the molar surface enthalpy ensures that the surface energies retain their values reported.

The atomic density $n_{i(M)}^{surf}$ of element *i* is obtained by summation of the surface area $a_{i,surf}$ and the subsurface area $a_{i,sub}$:

$$n_{i(M)}^{surf} = \frac{a_{i,surf} + a_{i,sub}}{\pi r_{i(M)}^2} \tag{A1}$$

in which $a_{i(M)} = \pi r_{i(M)}^2$ the atomic cross section with $r_{i(M)}$ the atomic radius of one atom *i* of material *M*.

The surface fraction $x_{i(M)}^{surf}$ of atoms *i* at surface *M* in Eq. (5) relates to all atomic species including a fraction $x_{void(M)}^{surf}$ of the area, devoid of atoms, that does not participate in chemical interaction. For a unit area *A* the surface fraction covered by atom *i* at surface *M* is:

$$x_{i(M)}^{surf} = \frac{A_{i(M)}}{A} = \frac{a_{i(M)} n_{i(M)}^{surf} N_A}{A} \tag{A2}$$

where $A_{i(M)}$ is the area covered by i with $a_{i(M)}$ the atomic surface in cross section and N_A Avogadro's number. The surface fractions add up to unity for every side of the interface according to:

$$\sum x_{i(M)}^{surf} + x_{void(M)}^{surf} = 1. \tag{A3}$$

Then, the cross sections of the atoms that make up the surface (and subsurface) layer at either side of the interface.

The intersections of the atomic cross sections projected are equal to the product of surface fractions $x_{i(M)}^{surf} x_{j(N)}^{surf}$ of Eq. (4). If an atom is opposed by empty space then the solution enthalpy is, of course, zero.

Appendix B: Macroscopic Atom Model

In the macroscopic atom model (MAM) [35] the atoms are represented as simple thermodynamic units. Originally, the MAM was constructed to predict properties of binary alloys. Their main mode of interactions of the atomic building blocks is constituted by their macroscopic influence on electrons. An attractive potential φ^* is derived from the work function of the elemental material and has the properties of electronegativity. The densities of outer electrons n_{WS} that are at the Wigner-Seitz perimeter of the atomic unit are thought to constitute a repulsive force toward neighboring atoms. The electron density was found to correspond to the bulk modulus via the following relation:

$$n_{WS}^2 = B / V_m \tag{B1}$$

and has arbitrary units. Chemical interactions are taken into account via a constant term R_{hybr} which is by its nature attractive. When an element belongs to the non-metalloids, a so-called transformation enthalpy ΔH^{trans} is required to transform the element to a hypothetical metal state. The interaction between one atomic unit *A* completely surrounded by material *B* is then computed with:

$$\Delta H_{AB}^{sol} = \frac{P V_{m,A}^{2/3}}{\left(\frac{1}{n_{WS}^{1/3}}\right)_{avg}} \left[-\left(\Delta\varphi^*\right)^2 + Q\left(\Delta n_{WS}^{1/3}\right)^2 - R_{hybr} \right] + \Delta H_A^{trans} \tag{B2}$$

Values for φ^*, n_{WS}, V_m and ΔH^{trans} are specified for each element and tabulated [35]. The constant *Q* has a value of 9.4 (volt^2/density unit$^{2/3}$). The constant *P* depends on the combination of elements and their valences and takes the values of 14.2 (both elements have valence higher than 2), 10.7 (both elements are mono-valent, di-valent or a combination thereof) and 12.35 when the binary mixture is composed of both type of elements. The constant R_{hybr} has been attributed to hybridization effects and is tabulated [35] as well for each element. When the hybridization constant R_{hybr} is unity for both elements, the product reduces

to zero. The molar volume of both elements is allowed to change to describe the redistribution of electrical charge when two elements form an alloy. The volume change is driven by the difference of electronegativity $\Delta\varphi^*$:

$$V_{m,\,alloy}^{2/3}(A) = V_{m,\,pure}^{2/3}(A)\left(1 + a_A\left(\varphi_A^* - \varphi_B^*\right)\right) \tag{B3}$$

in which a_A is an atomic constant and is also tabulated [35].

The MAM permits adaptation of the molar volume due to electronegativity differences for binary substances only; see Eq. (B3). However, for a compound containing *n* different elements the molar volume of atom *i* is estimated with geometric average of the molar volume $V_{m,ik}^{2/3}$ of all binary pairs i,k with $i \neq k$, thus:

$$V_{m,i}^{2/3} = \left(\prod_{i=1}^{n-1} V_{m,ik}^{2/3}\right)^{1/(n-1)} . \tag{B4}$$

The radii r_i of the atoms present in the bulk phases are derived from the molar volumes obtained from Eq. (B4) assuming a densely packed structure. At this point the molar fractions are determined; see Eqs (6), (7), (12) and (13).

Acknowledgements

The authors gratefully acknowledge the financial support of the German Research Foundation (Deutsche Forschungsgemeinschaft, DFG, SPP 1568, SL184/1-2). We are indebted to Professor Jochen M. Schneider and Dr. Lin Shang (RWTH Aachen University) for stimulating discussions.

References

[1] M.W. Barsoum, T. El-Raghy, The MAX phases: Unique new carbide and nitride materials - Ternary ceramics turn out to be surprisingly soft and machinable, yet also heat-tolerant, strong and lightweight, Am Sci, 89 (2001) 334-343.
[2] M.W. Barsoum, The M(N+1)AX(N) phases: A new class of solids; Thermodynamically stable nanolaminates, Prog Solid State Ch, 28 (2000) 201-281.
[3] M.W. Barsoum, Physical Properties of the MAX Phases, in: K.H.J.B. Editors-in-Chief: W.C. Robert, C.F. Merton, I. Bernard, J.K. Edward, M. Subhash, V. Patrick (Eds.) Encyclopedia of Materials: Science and Technology (Second Edition), Elsevier, Oxford, 2006, pp. 1-11.
[4] Z.J. Lin, M.S. Li, J.Y. Wang, Y.C. Zhou, High-temperature oxidation and hot corrosion of Cr2AlC, Acta Mater, 55 (2007) 6182-6191.
[5] L.O. Xiao, S.B. Li, G.M. Song, W.G. Sloof, Synthesis and thermal stability of Cr2AlC, J Eur Ceram Soc, 31 (2011) 1497-1502.
[6] D.B. Lee, T.D. Nguyen, S.W. Park, Long-Time Oxidation of Cr2AlC Between 700 and 1,000 degrees C in Air, Oxid Met, 77 (2012) 275-287.
[7] G.M. Song, V. Schnabel, C. Kwakernaak, S. Van der Zwaag, J.M. Schneider, W.G. Sloof, High temperature oxidation behaviour of Ti2AlC ceramic at 1200 degrees C, Mater High Temp, 29 (2012) 205-209.
[8] S. Gupta, M.W. Barsoum, Synthesis and oxidation of V2AlC and (Ti-0.5, V-0.5)(2)AlC in air, J Electrochem Soc, 151 (2004) D24-D29.
[9] M.W. Barsoum, H.I. Yoo, I.K. Polushina, V.Y. Rud, Y.V. Rud, T. El-Raghy, Electrical conductivity, thermopower, and hall effect of Ti(3)AIC(2), Ti(4)AIN(3), and Ti3SiC2, Phys Rev B, 62 (2000) 10194-10198.
[10] M. Haftani, M.S. Heydari, H.R. Baharvandi, N. Ehsani, Studying the oxidation of Ti2AlC MAX phase in atmosphere: A review, Int J Refract Met H, 61 (2016) 51-60.
[11] G.M. Song, Y.T. Pei, W.G. Sloof, S.B. Li, J.T.M. De Hosson, S. van der Zwaag, Oxidation-induced crack healing in Ti3AlC2 ceramics, Scripta Mater, 58 (2008) 13-16.
[12] S.B. Li, G.M. Song, K. Kwakernaak, S. van der Zwaag, W.G. Sloof, Multiple crack healing of a Ti2AlC ceramic, J Eur Ceram Soc, 32 (2012) 1813-1820.
[13] S.B. Li, L.O. Xiao, G.M. Song, X.M. Wu, W.G. Sloof, S. van der Zwaag, Oxidation and Crack Healing Behavior of a Fine-Grained Cr2AlC Ceramic, J Am Ceram Soc, 96 (2013) 892-899.
[14] A.S. Farle, C. Kwakernaak, S. van der Zwaag, W.G. Sloof, A conceptual study into the potential of M(n+1)AX(n)-phase ceramics for self-healing of crack damage, J Eur Ceram Soc, 35 (2015) 37-45.
[15] L. Shen, D. Eichner, S. van der Zwaag, C. Leyens, W.G. Sloof, Reducing the erosive wear rate of Cr2AlC MAX phase ceramic by oxidative healing of local impact damage, Wear, 358-359 (2016) 1-6.
[16] W.G. Sloof, R. Pei, S.A. McDonald, J.L. Fife, L. Shen, L. Boatemaa, A.S. Farle, K. Yan, X. Zhang, S. van der Zwaag, P.D. Lee, P.J. Withers, Repeated crack healing in MAX-phase ceramics revealed by 4D in situ synchrotron X-ray tomographic microscopy, Sci Rep, 6 (2016) 23040.
[17] J.L. Smialek, Oxidation of Al2O3 Scale-Forming MAX Phases in Turbine Environments, Metall Mater Trans A, 49a (2018) 782-792.
[18] G.M. Song, S.B. Li, C.X. Zhao, W.G. Sloof, S. van der Zwaag, Y.T. Pei, J.T.M. de Hosson, Ultra-high temperature ablation behavior of Ti2AlC ceramics under an oxyacetylene flame, J Eur Ceram Soc, 31 (2011) 855-862.

[19] A.S.M. Farle, J. Stikkelman, S. van der Zwaag, W.G. Sloof, Oxidation and self-healing behaviour of spark plasma sintered Ta2AlC, J Eur Ceram Soc, 37 (2017) 1969-1974.
[20] I.J. Bennett, J.M. Kranenburg, W.G. Sloof, Modeling the influence of reactive elements on the work of adhesion between oxides and metal alloys, J Am Ceram Soc, 88 (2005) 2209-2216.
[21] H.J. Yang, Y.T. Pei, J.C. Rao, J.T.M. De Hosson, S.B. Li, G.M. Song, High temperature healing of Ti2AlC: On the origin of inhomogeneous oxide scale, Scripta Mater, 65 (2011) 135-138.
[22] J.C. Rao, Y.T. Pei, H.J. Yang, G.M. Song, S.B. Li, J.T.M. De Hosson, TEM study of the initial oxide scales of Ti2AlC, Acta Mater, 59 (2011) 5216-5223.
[23] H.J. Yang, Y.T. Pei, J.T.M. De Hosson, Oxide-scale growth on Cr2AlC ceramic and its consequence for self-healing, Scripta Mater, 69 (2013) 203-206.
[24] L. Shang, P.K. Gokuldoss, S. Sandlobes, M.T. Baben, J.M. Schneider, Effect of Si additions on the Al2O3 grain refinement upon oxidation of Cr2AlC MAX phase, J Eur Ceram Soc, 37 (2017) 1339-1347.
[25] R. Pei, S.A. McDonald, L. Shen, S. van der Zwaag, W.G. Sloof, P.J. Withers, P.M. Mummery, Crack healing behaviour of Cr2AlC MAX phase studied by X-ray tomography, J Eur Ceram Soc, 37 (2017) 441-450.
[26] B.X. Wang, A.G. Zhou, Q.K. Hu, L.B. Wang, Synthesis and oxidation resistance of V2AlC powders by molten salt method, Int J Appl Ceram Tec, 14 (2017) 873-879.
[27] D.P. Sigumonrong, J. Zhang, Y.C. Zhou, D. Music, J. Emmerlich, J. Mayer, J.M. Schneider, Interfacial structure of V2AlC thin films deposited on (11(2)over-bar0)-sapphire, Scripta Mater, 64 (2011) 347-350.
[28] D.J. Siegel, L.G. Hector, J.B. Adams, Adhesion, stability, and bonding at metal/metal-carbide interfaces: Al/WC, Surf Sci, 498 (2002) 321-336.
[29] D.J. Siegel, L.G. Hector, J.B. Adams, Ab initio study of Al-ceramic interfacial adhesion, Phys Rev B, 67 (2003).
[30] J.M. Howe, Bonding, Structure, and Properties of Metal-Ceramic Interfaces .2. Interface Fracture-Behavior and Property Measurement, International Materials Reviews, 38 (1993) 257-271.
[31] L.P.H. Jeurgens, W.G. Sloof, F.D. Tichelaar, E.J. Mittemeijer, Thermodynamic stability of amorphous oxide films on metals: Application to aluminum oxide films on aluminum substrates, Phys Rev B, 62 (2000) 4707-4719.
[32] L.P.H. Jeurgens, W.G. Sloof, F.D. Tichelaar, E.J. Mittemeijer, Structure and morphology of aluminium-oxide films formed by thermal oxidation of aluminium, Thin Solid Films, 418 (2002) 89-101.
[33] E.A. Guggenheim, Statistical Thermodynamics of Co-Operative Systems (a Generalization of the Quasi-Chemical Method), Transactions of the Faraday Society, 44 (1948) 1007-1012.
[34] J. Ganguly, Chapter 3. Thermodynamic modelling of solid solution European Mineralogical Union notes in mineralogy, European Mineralogical Union2001.
[35] F.R. de Boer, Boom, R., Mattens, W.C. M., Miedema, A. R., Niessen, A. K., Cohesion in Metals: Transition Metal Alloys. Vol. 1 Elsevier Science Publishers B.V., Amsterdam, North Holland, 1989.
[36] L. Vitos, A.V. Ruban, H.L. Skriver, J. Kollar, The surface energy of metals, Surf Sci, 411 (1998) 186-202.
[37] S.H. C. Creemers, J. Luyten, M. Schurmans, Synergy between Material, Surface Science, Experiments and Simulations., in: R.D.N. Guillermo Bozzolo, Phillip B. Abel. (Ed.) Applied Computational Materials Modeling: Theory, Simulation and Experiment, Springer, New York, NY, 2007, pp. xvi, 491 p.

[38] B.S. Bokshteĭn, M.I. Mendelev, D.J. Srolovitz, Thermodynamics and kinetics in materials science : a short course, Oxford University Press, New York, 2005.
[39] P.I. Loeff, A.W. Weeber, A.R. Miedema, Diagrams of Formation Enthalpies of Amorphous-Alloys in Comparison with the Crystalline Solid-Solution, Journal of the Less-Common Metals, 140 (1988) 299-305.
[40] M.S. Mousavi, R. Abbasi, S.F. Kashani-Bozorg, A Thermodynamic Approach to Predict Formation Enthalpies of Ternary Systems Based on Miedema's Model, Metall Mater Trans A, 47a (2016) 3761-3770.
[41] Q.T. Guo, O.J. Kleppa, The standard enthalpies of formation of the compounds of early transition metals with late transition metals and with noble metals as determined by Kleppa and co-workers at the University of Chicago - A review, J Alloy Compd, 321 (2001) 169-182.
[42] Y. Ouyang, X.P. Zhong, Y. Du, Y.P. Feng, Y.H. He, Enthalpies of formation for the Al-Cu-Ni-Zr quaternary alloys calculated via a combined approach of geometric model and Miedema theory, J Alloy Compd, 420 (2006) 175-181.
[43] Y.F. Ouyang, X.P. Zhong, Y. Du, Z.P. Jin, Y.H. He, Z.H. Yuan, Formation enthalpies of Fe-Al-RE ternary alloys calculated with a geometric model and Miedema's theory, J Alloy Compd, 416 (2006) 148-154.
[44] J. Abrahamson, The surface energies of graphite, Carbon, 11 (1973) 337-362.
[45] H. Zaidi, F. Robert, D. Paulmier, Influence of Adsorbed Gases on the Surface-Energy of Graphite - Consequences on the Friction Behavior, Thin Solid Films, 264 (1995) 46-51.
[46] S.G.T.E. (SGTE), Thermodynamic Properties of Inorganic Materials compiled by SGTE, in: P.J.S. I. Hurtado and D. Neuschütz (Ed.) Subvolume A

Pure Substances

Heat Capacities, Enthalpies, Entropies and Gibbs Energies, Phase Transition Data, Springer-Verlag, Berlin Heidelberg New York, 1999.
[47] W.W. Gerberich, M.J. Cordill, Physics of adhesion, Reports on Progress in Physics, 69 (2006) 2157-2203.
[48] F. Reichel, L.P.H. Jeurgens, E.J. Mittemeijer, Thermodynamic model of oxide overgrowth on bare metals: Relaxation of growth strain by plastic deformation, Phys Rev B, 74 (2006).
[49] M.W. Barsoum, MAX phases : properties of machinable ternary carbides and nitrides, Wiley-VCH Verlag GmbH & Co. KGaA, Weinheim, Germany, 2013, pp. xiv, 421 pages.
[50] B. Liu, J.Y. Wang, J. Zhang, J.M. Wang, F.Z. Li, Y.C. Zhou, Theoretical investigation of A-element atom diffusion in Ti(2)AC (A=Sn, Ga, Cd, In, and Pb), Appl Phys Lett, 94 (2009).
[51] J. Wang, J. Wang, Y. Zhou, Stable M2AlC(0001) surfaces (M = Ti, V and Cr) by first-principles investigation, Journal of Physics: Condensed Matter, 20 (2008) 225006.
[52] M.W. Barsoum, M. Radovic, Elastic and Mechanical Properties of the MAX Phases, Annual Review of Materials Research, Vol 41, 41 (2011) 195-227.
[53] J.L. Smialek, Oxygen diffusivity in alumina scales grown on Al-MAX phases, Corros Sci, 91 (2015) 281-286.
[54] J.C. Schuster, H. Nowotny, C. Vaccaro, The Ternary-Systems - Cr-Al-C,V-Al-C, and Ti-Al-C and the Behavior of H-Phases (M2alc), Journal of Solid State Chemistry, 32 (1980) 213-219.
[55] H. Graafsma, M. Souhassou, A. Puig-Molina, S. Harkema, A. Kvick, C. Lecomte, Towards extinction-free experimental diffraction data on Al2O3, Acta Crystallographica Section B-Structural Science, 54 (1998) 193-195.

Figure Captions

Figure 1. The interface constructed on the left between material *M* (blue and gray atoms) and material *N* (red and black atoms) is folded open to expose both sides of the interface in the middle. When both surfaces are merged the intersection of atomic cross sections (at the right) can be determined to obtain the interaction enthalpy per atomic pair *ij* per unit surface.

Figure 2. The interface of the system α-Al_2O_3 [11-20](1-100) // M_2AlC [0001](11-20) with the divides where the interface energies are calculated. The interface used to compute the work of adhesion W_{ad} is indicated by a gray line. The interfaces used to calculate the work of cohesion W_{coh} are indicated with black lines (one example for both materials).

Table 1. The lattice parameters of the materials used in the calculations.

Lattice parameters	Ti_2AlC [54]	V_2AlC [54]	Cr_2AlC [54]	Al_2O_3 [55]
a (Å)	3.052	2.9116	2.854	4.757
b (Å)	3.052	2.9116	2.854	4.757
c (Å)	13.64	13.14	12.82	12.9877
α	90°	90°	90°	90°
β	90°	90°	90°	90°
γ	120°	120°	120°	120°

Table 2. The interaction energy and surface energies of both sides of the interface contribute to the cohesive energy W_{coh} between crystallographic planes in a single compound.

Side 1	Side 2	γ_1^{surf} (J/m²)	γ_2^{surf} (J/m²)	$\gamma_{12}^{interaction}$ (J/m²)	W_{coh} (J/m²)
Ti_2AlC (0001)-C	Ti_2AlC (0001)-Ti	2.1	2.4	1.5	6.0
V_2AlC (0001)-C	V_2AlC (0001)-V	1.9	2.3	1.5	5.8
Cr_2AlC (0001)-C	Cr_2AlC (0001)-Cr	1.8	2.2	0.7	4.7
Ti_2AlC (0001)-Al	Ti_2AlC (0001)-Ti	1.6	2.1	0.9	4.6
V_2AlC (0001)-Al	V_2AlC (0001)-V	1.5	1.9	1.3	4.7
Cr_2AlC (0001)-Al	Cr_2AlC (0001)-Cr	1.5	1.8	0.5	3.7
Al_2O_3 (11-20)-O	Al_2O_3 (11-20)-O *	1.5	1.5	3.6	6.7

**) Note that the oxygen atoms interact with the aluminum atoms of the opposite layer*

Table 3. The work of adhesion between a MAX phase material M_2AlC (M = Ti, V, Cr) and α-Al_2O_3 depends on the surface termination of the MAX phase. α-Al_2O_3 is terminated by low density oxygen atoms.

Side 1	Side 2	γ_1^{surf} (J/m²)	γ_2^{surf} (J/m²)	$\gamma_{12}^{interaction}$ (J/m²)	W_{ad} (J/m²)
Ti_2AlC (0001) –(Al)– Ti	Al_2O_3 (11-20)-(Al)-O	2.1	1.5	3.4	7.0
V_2AlC (0001) –(Al)– V	Al_2O_3 (11-20)-(Al)-O	1.9	1.5	3.0	6.8
Cr_2AlC (0001) –(Al)– Cr	Al_2O_3 (11-20)-(Al)-O	1.8	1.5	2.5	5.8
Ti_2AlC (0001) –(Ti)– Al	Al_2O_3 (11-20)-(Al)-O	1.6	1.5	3.0	6.1
V_2AlC (0001) –(V)– Al	Al_2O_3 (11-20)-(Al)-O	1.5	1.5	3.3	6.3
Cr_2AlC (0001) –(Cr)– Al	Al_2O_3 (11-20)-(Al)-O	1.5	1.5	3.4	6.4
Ti_2AlC (0001) –(Ti)–C	Al_2O_3 (11-20)-(Al)-O	2.4	1.5	1.7	5.6
V_2AlC (0001) –(V)– C	Al_2O_3 (11-20)-(Al)-O	2.3	1.5	1.5	5.3
Cr_2AlC (0001) –(Cr)– C	Al_2O_3 (11-20)-(Al)-O	2.2	1.5	1.2	5.0

Table 4. The cohesive energy of the (11-20)-planes of the MAX phase materials M_2AlC (M = Ti, V, Cr).

Side 1	Side 2	γ_1^{surf} (J/m²)	γ_2^{surf} (J/m²)	$\gamma_{12}^{interaction}$ (J/m²)	W_{coh} (J/m²)
Ti_2AlC (11-20)	Ti_2AlC (11-20)	2.1	2.1	0.1	4.3
V_2AlC (11-20)	V_2AlC (11-20)	2.0	2.0	0.3	4.3
Cr_2AlC (11-20)	Cr_2AlC (11-20)	3.0	3.0	0.4	6.5

Table 5. The work of adhesion of the (11-20)-planes of the MAX phase materials M_2AlC (M = Ti, V, Cr) with α-Al_2O_3.

Side 1	Side 2	γ_1^{surf} (J/m²)	γ_2^{surf} (J/m²)	$\gamma_{12}^{interaction}$ (J/m²)	W_{ad} (J/m²)
Ti_2AlC (11-20)	Al_2O_3 (11-20)-(Al)-O	2.1	1.5	2.6	5.9
V_2AlC (11-20)	Al_2O_3 (11-20)-(Al)-O	2.0	1.5	2.4	6.7
Cr_2AlC (11-20)	Al_2O_3 (11-20)-(Al)-O	3.0	1.5	2.1	6.7